Resonant excitations of single and two-qubit systems coupled to a tank circuit

S. N. Shevchenko,[1] S. H. W. van der Ploeg,[2] M. Grajcar,[2,3] E. Il'ichev,[2] A. N. Omelyanchouk,[1] and H.-G. Meyer[2]

[1]*B. Verkin Institute for Low Temperature Physics and Engineering, 47 Lenin Avenue, 61103 Kharkov, Ukraine*

[2]*Institute of Photonic Technology, P.O. Box 100239, D-07702 Jena, Germany*

[3]*Department of Experimental Physics, Comenius University, SK-84248 Bratislava, Slovakia*

The interaction of flux qubits with a low-frequency tank circuit is studied. It is shown that changes in the state of the interacting qubits influence the effective inductance and resistance of the circuit, which is the essence of the so-called impedance measurement technique. The multiphoton resonant excitations in both single flux qubits and pairs of coupled flux qubits are investigated. In particular, we compare our theoretical results with recent spectroscopy measurements, Landau-Zener interferometry, and the multiphoton fringes.

I. INTRODUCTION

Quantum properties of the atom-photon interaction have been mainly a subject of quantum optics and atomic physics. For example, the interaction between an atom and a photon was studied by experiments with a single atom in a cavity; this topic represents a textbook subject of quantum electrodynamics.[1] Recently a similar configuration has been realized for superconducting quantum circuits[2] where Josephson qubits play the role of atoms, while a microwave resonator replaces the cavity. Usually for such kind of experiments the photon energy is close to the level separation Δ/h of the atom or qubit. In contrast, in the experiments of Refs. 3–9, driven qubits are coupled to a *LC* tank circuit with a resonance frequency well below the level splitting of the qubits. In particular, our study here is motivated by the recent experiments[8] where driven one or two flux qubits systems were inductively coupled to a low-frequency superconducting tank circuit.

The flux, or persistent current, qubit is a superconducting ring with three Josephson junctions.[10] The circuit is characterized by a two-dimensional potential which, for suitable qubit and external parameters, exhibits two minima. If the applied magnetic flux is half of a flux quantum, these minima have equal energies. In the flux neighborhood of this point the degeneracy is lifted due to finite tunneling probability between minima. Therefore, the circuit forms an effective two-level quantum system.

Strictly speaking a system of qubits coupled to a resonant circuit should be treated quantum mechanically, as in Refs. 9 and 11–14. However, due to the weak coupling of the qubits to the classical circuit, the qubit-oscillator system can be treated semiclassically.[15–19] In this paper we study the impact of the qubits on the tank circuit in terms of the effective inductance and resistance of the tank. We show that in some limiting cases, the analyzed equations can be simplified resulting in a more transparent description of the behavior of the investigated qubit system.

In this paper we will address the measurement with the resonant tank circuit in three different driving regimes of the qubits: in the ground state (without driving field) and in the weakly and strongly driven regimes. Such regimes are useful for controlling the state of the qubit with the driving field.

Particularly interesting is the strongly driven regime, where due to the interference between different Landau-Zener (LZ) tunneling events the state of the system quasiperiodically depends on both the dc bias and the ac driving amplitude.[20–24] Motivated by our experimental paper,[8] we study the measurement technique in application to both single and coupled flux qubits. Systems of coupled qubits have been studied previously[25] as well as spectroscopy with switching current readout.[26,27] The study of the dynamical driving of coupled qubits is important to form an entangled state (in particular, preparation of maximally entangled Bell states) and to perform two-qubit operations, such as a controlled-NOT (C-NOT) gate.[28,29] Particularly, we study the multiphoton resonances in a two-qubit four-level system. This is analogous to the resonances studied in Ref. 30 where a multilevel system based on a single flux qubit including the upper levels was considered.

The remainder of this paper is organized as follows. In Sec. II we derive equations which describe the influence of the qubits on the tank circuit in terms of the effective inductance and resistance. Limiting cases are considered in Sec. III for a single flux qubit coupled to the tank circuit. In Sec. IV equations for the coupled qubits system are formulated. Numerically calculated results are presented in Secs. V and VI for single and coupled qubits, respectively. Experimental results for the multiphoton resonances in single flux qubit are shown in Sec. VII.

II. DESCRIPTION OF THE MEASUREMENT WITH TANK CIRCUIT

Consider a tank circuit which consists of an inductor L_T, a capacitor C_T, and a resistor R_T connected in parallel (see Fig. 1). The voltage V in the current-biased tank circuit ($I_{bias} = I_A \sin \omega_{rf} t$), which is pierced by the external flux Φ_e, is described by the following nonlinear equation:[19]

$$C_T \ddot{V} + \frac{\dot{V}}{R_T} + \frac{V}{L_T} = -\frac{\dot{\Phi}_e(V, \dot{V})}{L_T} + \dot{I}_{bias}. \tag{1}$$

The external flux Φ_e is assumed to be proportional to the coupling parameter k^2 and to depend on time via voltage V and its derivative $\dot{V}$.[31]
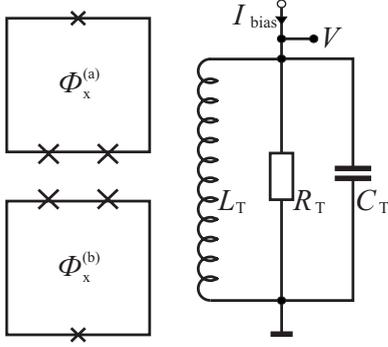
FIG. 1. Two-qubit system coupled to a tank circuit. The flux qubits are pierced by magnetic fluxes $\Phi_x^{(a,b)}$ induced by the currents in the controlling coils (not shown in the scheme) and by the current in the tank inductor. The qubits are coupled to each other and to the tank circuit. The resonant tank circuit consists of the inductor L_T, capacitor C_T, and resistor R_T; the circuit is biased with a rf current I_{bias}. The tank voltage V is the measurable value.

The stationary oscillations in the nonlinear system described by Eq. (1) can be reduced to oscillations in a linear system by making use of the Krylov-Bogolyubov technique of asymptotic expansion.[31] Specifically, in the first-order approximation with respect to the coupling parameter k^2 and close to the principal resonance ($\omega_{\text{rf}} \approx \omega_T \equiv 1/\sqrt{L_T C_T}$), the equivalent linear system is characterized by the effective resistance R_{eff} and inductance L_{eff} as follows:[31]

$$C_T \ddot{V} + \frac{\dot{V}}{R_{\text{eff}}} + \frac{V}{L_{\text{eff}}} = \dot{I}_{\text{bias}}, \tag{2}$$

$$V = v \cos(\omega_{\text{rf}} t + \alpha), \tag{3}$$

$$\frac{1}{R_{\text{eff}}(v)} = \frac{1}{R_T}[1 - Q\beta_s(v)], \tag{4}$$

$$\frac{1}{L_{\text{eff}}(v)} = \frac{1}{L_T}[1 + \beta_c(v)], \tag{5}$$

where $Q = \omega_T C_T R_T$ is the quality factor of the unloaded tank circuit (at $\Phi_e = 0$) and the functions $\beta_{s,c}(v)$ are given by

$$\begin{Bmatrix} \beta_s(v) \\ \beta_c(v) \end{Bmatrix} = \frac{1}{\pi v} \int_0^{2\pi} \dot{\Phi}_e(v \cos \psi, -v \omega_{\text{rf}} \sin \psi) \begin{Bmatrix} \sin \psi \\ \cos \psi \end{Bmatrix} d\psi. \tag{6}$$

Let us also introduce the notations $\varkappa_{s,c}$ for the partial derivatives,

$$\dot{\Phi}_e(V, \dot{V}) = \frac{\partial \Phi_e}{\partial V} \dot{V} + \frac{\partial \Phi_e}{\partial \dot{V}} \ddot{V}$$

$$\equiv \varkappa_s(v, \psi) v \sin \psi + \varkappa_c(v, \psi) v \cos \psi, \tag{7}$$

where $\psi = \omega_{\text{rf}} t + \alpha$. If $\varkappa_{s,c}(v, \psi)$ are functions of either $\sin \psi$ or $\cos \psi$ only, i.e., $\varkappa_{s,c}(v, \psi) = \varkappa'_{s,c}(v, \sin \psi)$ or $\varkappa_{s,c}(v, \psi) = \varkappa'_{s,c}(v, \cos \psi)$, Eq. (6) leads to a simpler form for $\beta_{s,c}$,

$$\beta_s(v) = \frac{1}{\pi} \int_0^{2\pi} \varkappa_s(v, \psi) \sin^2 \psi d\psi, \tag{8}$$

$$\beta_c(v) = \frac{1}{\pi} \int_0^{2\pi} \varkappa_c(v, \psi) \cos^2 \psi d\psi. \tag{9}$$

As a result of Eqs. (2) and (5) the resonant frequency ω_{eff} becomes amplitude dependent and is shifted by

$$\frac{\omega_{\text{eff}}(v) - \omega_T}{\omega_T} = \frac{1}{2} \beta_c(v). \tag{10}$$

The phase shift α and amplitude v depend on the frequency detuning $\xi_0 \equiv \frac{\omega_T - \omega_{\text{rf}}}{\omega_T}$ and the qubit state (via $\beta_{s,c}$). In the stationary regime they are given by

$$\begin{cases} v = I_A R_{\text{eff}} \cos \alpha, \\ \tan \alpha = 2Q \dfrac{R_{\text{eff}}}{R_T}\left(\xi_0 + \dfrac{L_T - L_{\text{eff}}}{2L_T}\right), \end{cases} \tag{11}$$

which can be rewritten in terms of the effective quality factor Q_{eff} and effective frequency shift ξ_{eff}:

$$\begin{cases} v\sqrt{1 + 4Q_{\text{eff}}^2 \xi_{\text{eff}}^2} = \dfrac{I_A Q_{\text{eff}}}{\omega_T C_T}, \\ \tan \alpha = 2Q_{\text{eff}} \xi_{\text{eff}}, \end{cases} \tag{12}$$

$$Q_{\text{eff}}(v) = \omega_T C_T R_{\text{eff}}(v) = \frac{Q}{1 - Q\beta_s(v)}, \tag{13}$$

$$\xi_{\text{eff}}(v) = \xi_0 + \frac{1}{2}\beta_c(v) = \frac{\omega_{\text{eff}}(v) - \omega_{\text{rf}}}{\omega_T}. \tag{14}$$

Thus, the observable values—the amplitude v and the phase shift α—are defined by Eqs. (11) or (12), which depend on the response of the measurable system, $\Phi_e(V, \dot{V})$.

III. MEASUREMENT OF THE PERSISTENT CURRENT QUBIT

In this section we consider the system of the tank circuit coupled to a persistent current qubit with geometrical inductance L and average persistent current I_{qb}. The qubit is considered to be weakly coupled to the tank circuit via a mutual inductance M. As we discussed above, strictly speaking, the dynamics of the tank circuit has to be considered jointly with the dynamics of the qubit. However, in this section we consider two limiting cases, when the dynamics of the qubit can be treated separately from the dynamics of the tank circuit. For simplification we introduce phenomenologically the relaxation time T_1 (which can be caused by the tank as well) and consider the weak-coupling limit, $k^2 = \frac{M^2}{LL_T} \ll 1$.

A. Low-quality qubit ($T_1 \ll T$): Phase shift probes effective inductance of qubit

When all the qubit characteristic times, and in particular the relaxation time T_1, are smaller than the tank period T

$=2\pi/\omega_T$, the equations can be simplified since the equations for the tank voltage can be averaged over the fast oscillating terms. This averaging is assumed henceforth for all values in this subsection. Then the time derivative of the flux Φ_e, which is induced by the qubit in the tank circuit, can be described as

$$\dot{\Phi}_e = M\dot{I}_{qb} = M\frac{\partial I_{qb}}{\partial \Phi}\dot{\Phi}, \qquad (15)$$

where $\Phi = \Phi_{dc} + MI_L$ is the flux in the qubit loop (here[19] we ignore the small self-induced flux $-LI_{qb}$), which consists of the time-independent part Φ_{dc} and of the flux induced by the current I_L in the tank inductor. This can be rewritten by introducing the (inverse) effective inductance of the qubit, $\mathcal{L}^{-1} = \frac{\partial I_{qb}(\Phi)}{\partial \Phi}$, and the inductance value, which characterizes the response of the qubit, $\tilde{L} = M^2 \mathcal{L}^{-1}$. Then it follows:

$$\dot{\Phi}_e = \tilde{L}(I_L)\dot{I}_L; \qquad (16)$$

and for the tank voltage we have[19]

$$V = L_T\dot{I}_L - \dot{\Phi}_e = [L_T - \tilde{L}(I_L)]\dot{I}_L. \qquad (17)$$

Since $\tilde{L} \propto k^2$ and $\tilde{L} \ll L_T$, in the first approximation in k^2 we can insert I_L in the right-hand side of Eq. (16) found from the above equation,

$$I_L(t) \approx \frac{1}{L_T}\int V dt = \frac{v}{\omega_T L_T}\sin(\omega_{rf}t + \alpha). \qquad (18)$$

Then by Eqs. (7)–(9) we have

$$\beta_s = 0, \quad \beta_c = \frac{1}{\pi}\int_0^{2\pi} k^2 L\mathcal{L}^{-1}(v,\psi)\cos^2\psi d\psi, \qquad (19)$$

where the qubit effective inductance is defined by the total flux Φ, piercing the qubit loop,

$$\mathcal{L}^{-1}(v,\psi) \equiv \left.\frac{\partial I_{qb}(\Phi)}{\partial \Phi}\right|_{\Phi = \Phi_{dc} + M/(L_T\omega_T)v\sin\psi}. \qquad (20)$$

It follows:

$$\tan\alpha \approx 2Q\xi_0 + Q\beta_c, \quad v \approx I_A R_T\cos\alpha. \qquad (21)$$

Actually, this is a generalization of the result of Ref. 17 for the case when the qubit can be in the excited state (which is taken into account by the expectation value of the current I_{qb}).

If the bias current amplitude I_A is small enough to be ignored in Eq. (20), where $v \sim I_A R_T$, then[19]

$$\tan\alpha \approx 2Q\xi_0 + k^2 Q\frac{L}{\mathcal{L}}, \quad v \approx I_A R_T\cos\alpha,$$

$$\mathcal{L}^{-1} \approx \frac{\partial I_{qb}(\Phi_{dc})}{\partial \Phi_{dc}}, \qquad (22)$$

which means that at the resonant frequency ($\xi_0 = 0$) the tank phase shift α is approximately proportional to the inverse inductance of the qubit $\mathcal{L}^{-1}$.

B. Higher-quality qubit ($T_1 \lesssim T$): Effective resistance due to qubit's lagging

Consider the case when the qubit relaxation time T_1 is of the same order as the tank period T (namely, $T_1 \lesssim T$). We assume exponential delayed response of the qubit, $1 - \exp(-t/T_1)$, which can be phenomenologically described as a qubit response lagging relative to the tank circuit (as, e.g., in Ref. 32). Therefore, Eq. (16) is replaced by

$$\dot{\Phi}_e(t) = \tilde{L}[I_L(t')]\dot{I}_L(t'), \qquad (23)$$

where $t' = t - T_1$ is the retarded time. Thus, the qubit response depends on the current in the tank $I_L = I_L(t')$, which is given by

$$I_L(t') \approx \frac{v}{\omega_T L_T}\sin(\omega_{rf}t' + \alpha)$$

$$= \frac{v}{\omega_T L_T}[C\sin(\omega_{rf}t + \alpha) - S\cos(\omega_{rf}t + \alpha)], \quad (24)$$

where $S = \sin(\omega_{rf}T_1)$ and $C = \cos(\omega_{rf}T_1)$. For the sake of simplicity we consider small bias current approximation, in this case Eqs. (23) and (24) and definitions (7)–(9) result in $\beta_s \approx k^2\frac{L}{\mathcal{L}}S$ and $\beta_c \approx k^2\frac{L}{\mathcal{L}}C$. Then, from Eqs. (4) and (5) one gets

$$\frac{L_T}{L_{eff}} \approx 1 + C \cdot k^2 Q\frac{L}{\mathcal{L}}, \qquad (25)$$

$$\frac{R_T}{R_{eff}} \approx 1 - S \cdot k^2 Q\frac{L}{\mathcal{L}}, \qquad (26)$$

$$\tan\alpha \approx \frac{2Q\xi_0 + C \cdot k^2 QL/\mathcal{L}}{1 - S \cdot k^2 QL/\mathcal{L}}, \qquad (27)$$

$$\frac{v}{I_A R_T} \approx \frac{\cos\alpha}{1 - S \cdot k^2 QL/\mathcal{L}}. \qquad (28)$$

Consider these expressions in the first approximation in $k^2 QL/\mathcal{L}$; for $\xi_0 = 0$ we obtain the following important result:

$$\tan\alpha \approx C \cdot k^2 QL/\mathcal{L},$$

$$\frac{v}{I_A R_T} \approx 1 + S \cdot k^2 QL/\mathcal{L}, \qquad (29)$$

which, in particular, shows that as $C \to 0$ there can be changes in the amplitude v without changes in the phase shift α as well as in the shift of the resonant frequency [Eq. (10)]. It is important to note that both the phase shift and amplitude are related to the qubit effective inductance $\mathcal{L}$, which explains their similar behavior in experiment. These equations might be useful for qualitative analysis of experimental results.

IV. COUPLED FLUX QUBITS

A. Hamiltonian

Close to its degeneracy point the flux qubit[10] can be described by the pseudospin Hamiltonian

$$H_{1qb} = -\frac{\Delta}{2}\sigma_1 - \frac{\epsilon(t)}{2}\sigma_3, \tag{30}$$

where the diagonal term ϵ is the energy bias, the off-diagonal term Δ is the tunneling amplitude between the wells (which corresponds to the definite directions of the current in the loop), and σ_j are Pauli matrices.

For the system of coupled qubits the effective Hamiltonian is

$$H_{2qbs} = \sum_{i=1,2} \left(-\frac{\Delta_i}{2}\sigma_1^{(i)} - \frac{\epsilon_i(t)}{2}\sigma_3^{(i)} \right) + \frac{J}{2}\sigma_3^{(1)}\sigma_3^{(2)}, \tag{31}$$

where J is the coupling energy between qubits, and $\sigma_1^{(i)}$ and $\sigma_3^{(i)}$ are the Pauli matrices in the basis $\{|\downarrow\rangle, |\uparrow\rangle\}$ of the current operator in the ith qubit, namely, $\sigma_a^{(1)} = \sigma_a \otimes \sigma_0$ and $\sigma_a^{(2)} = \sigma_0 \otimes \sigma_a$, where σ_0 is the unity matrix. The current operator is given by $I_i = -I_p^{(i)}\sigma_3^{(i)}$ with $I_p^{(i)}$ as the absolute value of the persistent current in the ith qubit; then the eigenstates of σ_3 correspond to the clockwise $(\sigma_3|\downarrow\rangle = -|\downarrow\rangle)$ and counterclockwise $(\sigma_3|\uparrow\rangle = |\uparrow\rangle)$ currents in the ith qubit. The tunneling amplitudes Δ_i are assumed to be constants. The biases $\epsilon_i = 2I_p^{(i)}\Phi_0 f^{(i)}(t)$ are controlled by the dimensionless magnetic fluxes $f^{(i)}(t) = \Phi_i/\Phi_0 - 1/2$ through the ith qubit. These fluxes consist of three components,

$$f^{(i)}(t) = f_i + \frac{M_i I_L}{\Phi_0} + f_{ac}\sin\omega t. \tag{32}$$

Here f_i is the adiabatically changing magnetic flux, experimentally applied by the coil and additional dc lines. The second term describes the flux induced by the current I_L in the tank coil, to which the ith qubit is coupled with the mutual inductance M_i. Moreover $f_{ac}\sin\omega t$ is the harmonic time-dependent component driving the qubit, typically applied by an on-chip microwave antenna.

B. Entanglement

It is convenient to present the density matrix for two qubits in the following form:

$$\rho = \frac{R_{\alpha\beta}}{4}\sigma_\alpha \otimes \sigma_\beta = \frac{R_{00}}{4}\sigma_0 \otimes \sigma_0 + \frac{R_{a0}}{4}\sigma_a \otimes \sigma_0 + \frac{R_{0b}}{4}\sigma_0 \otimes \sigma_b$$

$$+ \frac{R_{ab}}{4}\sigma_a \otimes \sigma_b, \tag{33}$$

which was shown to be suitable for both the definition and the calculation of the entanglement and other characteristics in multiqubit system.[28,33–35] Here $0 \le \{\alpha, \beta\} \le 3$ and $1 \le \{a, b\} \le 3$; the summation over twice repeating indices is assumed. The two vectors R_{a0} and R_{0b}, so-called coherence vectors or Bloch vectors, determine the properties of the individual qubits, while the tensor R_{ab} (the correlation tensor) accounts for the correlations.[33] [In the notations of Ref. 33, $\lambda_a(1) = R_{a0}$, $\lambda_b(2) = R_{0b}$, and $K_{ab} = R_{ab}$.] Following Ref. 33, we choose the measure of entanglement $\mathcal{E}$ to be the following:

$$\mathcal{E} = \frac{1}{3}\text{Tr}(M^T M), \quad M_{ab} = R_{ab} - R_{a0}R_{0b}. \tag{34}$$

This measure of entanglement fulfills certain reasonable requirements $(0 \le \mathcal{E} \le 1)$, in particular, $\mathcal{E} = 0$ for any product state and $\mathcal{E} = 1$ for any pure state with vanishing Bloch vectors R_{a0} and R_{0b}, corresponding to maximum entangled states (see Ref. 33 for more detail).

C. Liouville equation

The dynamics of the density matrix without taking into account the relaxation processes can be described by the Liouville equation: $i\dot\rho = [H, \rho]$, which is (generally speaking) a complex equation. We set both $\hbar = 1$ and $k_B = 1$ throughout. By the proper choice of the parametrization the Liouville equation can be written in the form of a system with a minimal number of real equations [3 for one qubit and 15 for two qubits).

To deal with the Liouville equation, we make use of the parametrization (decomposition) of the density matrix as described by Eq. (33). This allows one to benefit from the properties of the density matrix, namely, from its Hermiticity (then $R_{\alpha\beta}$ are real numbers) and from the normalization condition, $\text{Tr }\rho = 1$ (then $R_{00} = 1$). It follows that the density matrix is parametrized by 15 independent real values. It is useful to note that

$$\text{Tr}(\rho\sigma_a^{(1)}) = R_{a0}, \quad \text{Tr}(\rho\sigma_b^{(2)}) = R_{0b}. \tag{35}$$

After straightforward algebra the Liouville equation yields:

$$\dot{R}_{i0} = \varepsilon_{mni}B_m^{(1)}R_{n0} + \varepsilon_{3ni}JR_{n3},$$

$$\dot{R}_{0j} = \varepsilon_{mnj}B_m^{(2)}R_{0n} + \varepsilon_{3nj}JR_{3n},$$

$$\dot{R}_{ij} = \varepsilon_{mni}B_m^{(1)}R_{nj} + \varepsilon_{mnj}B_m^{(2)}R_{in} + \delta_{j3}\varepsilon_{3ni}JR_{n0} + \delta_{i3}\varepsilon_{3nj}JR_{0n}. \tag{36}$$

where $\mathbf{B}^{(i)}$ are "local magnetic fields," which for the flux qubits are defined as $\mathbf{B}^{(i)} = (-\Delta_i, 0, -\epsilon_i)$, and ε_{mni} is the Levi-Civita symbol.

D. Effective inductance of coupled qubits

For describing the effective inductance of coupled qubits it is important to note that the current in the ith qubit depends on the fluxes in both qubits, $I_{qb}^{(i)} = I_{qb}^{(i)}(\Phi_x^{(a)}, \Phi_x^{(b)})$. Here the fluxes $\Phi_x^{(a,b)}$ consist of a dc part, Φ_i, and of the flux generated by the current in the tank coil, I_L: $\Phi_x^{(i)} = \Phi_i + MI_L$. For simplicity we assume here that the qubit-tank mutual inductance M is the same for both qubits (for more detail, see Ref. 19). Then the time derivative is

$$\dot{I}_{qb}^{(i)} = \left(\frac{\partial}{\partial\Phi_x^{(a)}} + \frac{\partial}{\partial\Phi_x^{(b)}} \right) I_{qb}^{(i)}M\dot{I}_L. \tag{37}$$

In the limit of small bias current in the tank we can substitute Φ_i for $\Phi_x^{(i)}$ and define the qubit effective inductance with the
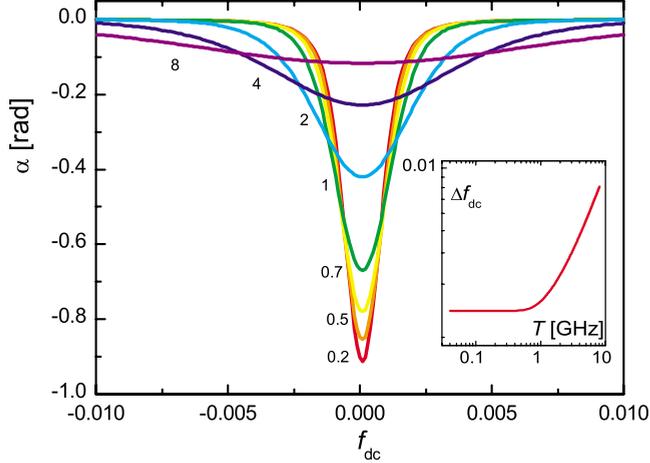
FIG. 2. (Color online) Influence of temperature on the ground-state measurement: the dependence of the tank phase shift on the flux detuning $f_{dc} = \Phi_{dc}/\Phi_0 - 1/2$ when the qubit is thermally excited. The numbers next to the curves stand for the temperature in gigahertz. Inset: temperature dependence of the width Δf_{dc} of the dip at half depth in the phase shift shown in the main panel.

symmetric change of the flux bias in both qubits[36] $\mathbf{\Phi}_x = (\Phi_a, \Phi_b)$,

$$\mathcal{L}_i^{-1} = \frac{\partial}{\partial \mathbf{\Phi}_x} I_{qb}^{(i)} \equiv \left(\frac{\partial}{\partial \Phi_a} + \frac{\partial}{\partial \Phi_b} \right) I_{qb}^{(i)}. \quad (38)$$

Then for the case of low-quality qubits, when their characteristic times are smaller than the tank period, analogously to Sec. III A, we obtain at the resonance frequency ($\xi_0 = 0$)

$$\tan \alpha \approx \sum_i \Xi_i \frac{\Phi_0}{I_p^{(i)}} \mathcal{L}_i^{-1}, \quad (39)$$

where we introduced the notation

$$\Xi_i = k^2 Q \frac{L_i I_p^{(i)}}{\Phi_0}. \quad (40)$$

V. RESULTS FOR SINGLE FLUX QUBIT

A. Spectroscopy

In Ref. [8] it was shown that the qubit parameters can be determined both by measurements in the ground state and by employing a spectroscopic measurement when the qubit is resonantly excited. In this section we show related numerically calculated graphs, making use of the results of Secs. II–IV.

Consider a qubit biased with a dc flux Φ_{dc} and driven with an ac flux $\Phi_{ac} \sin \omega t$, introducing

$$f_{dc} = \Phi_{dc}/\Phi_0 - 1/2 \quad \text{and} \quad f_{ac} = \Phi_{ac}/\Phi_0.$$

In order to get the effective inductance $\mathcal{L}$, as defined by Eq. (20), we have to calculate the average current in the qubit $I_{qb} = \langle I \rangle = \text{Tr}(\rho I)$, where $I = -I_p \sigma_3$ is the current operator defined by the amplitude I_p and the Pauli matrix σ_3. We calculate the reduced density matrix ρ with the Bloch equations,[7,37,38] which include phenomenological relaxation times, T_1 and T_2. It is convenient to express the density matrix in the energy representation $\rho = (1/2)(\tau_0 + X\tau_1 + Y\tau_2 + Z\tau_3)$, where τ_i are the Pauli matrices for this basis and τ_0 stands for the unity matrix. Z is equal to the difference between the populations of the ground and excited states. As a result the effective inductance is given by[19]

$$\mathcal{L}^{-1} = I_p \frac{\partial}{\partial \Phi} \left\{ \frac{\Delta}{\Delta E} X - \frac{2 I_p \Phi}{\Delta E} Z \right\}, \quad (41)$$

where $\Delta E = \sqrt{\Delta^2 + (2 I_p \Phi)^2}$.

First we consider the ground-state measurement, which is described by Eqs. (19)–(21). These equations not only allow us to reproduce the results of Refs. [17] and [39], valid for the case where the system is in the ground state, but also de-

FIG. 3. (Color online) Curves for a resonantly excited flux qubit: (a) the phase shift and (b) the amplitude of the tank voltage versus flux detuning f_{dc}. In panel (a) the numbers next to the curves stand for the driving amplitude f_{ac} multiplied by 1×10^3; in panel (b) the curves are for the amplitudes $f_{ac}(1 \times 10^3) = 1$, 1.5, and 3 from bottom to top.

TABLE I. The parameters used for plotting Fig. 3. Δ, $I_p\Phi_0$, Γ_1, and Γ_2 are tunneling amplitude, energy bias, relaxation rate, and dephasing rate, respectively. The Ξ describes the coupling between qubit and tank circuit. All parameters are in units of h GHz except Ξ which is dimensionless.

Δ	$I_p\Phi_0$	T	Γ_1	Γ_2	Ξ
3.5	700	1.4	0.7	0.7	2.6×10^{-3}

scribe the situation when the qubit is excited. Consider the influence of temperature when the qubit is in a thermal mixture of the ground and excited states. In this case $X=0$ and $Z=\tanh(\Delta E/2T)$. The resulting tank phase shift is shown in Fig. 2 for the following parameters:[39] $\Delta/h=2\times0.65$ GHz , $I_p\Phi_0/h=930$ GHz, $\omega_T/2\pi=32.675$ MHz, $LI_p/\Phi_0=0.0055$, $M/L=0.725$, $Q=725$, and $k=0.02$. The accurate account of Z allows us to describe the widening of the phase-shift dip, as shown in the inset of Fig. 2, which was reported in Ref. 39. The widening is due to the term that comes from differentiating the tanh in Eq. (41); this term becomes relevant for temperatures larger than $\Delta=1.3$ GHz and results in the exponential rise of the width for $T>T^*=\Delta\left[\frac{d}{dx}\tanh x\simeq 4\exp(-2x)\text{ at }x>1\right]$.

Now we consider the spectroscopical measurement, where the qubit is driven with the ac flux. In Fig. 3(a) we demonstrate the dependence of the phase shift α on the bias flux f_{dc} at $\omega_{rf}=\omega_T$ for different driving amplitudes at the driving frequency $\omega/2\pi=4.15$ GHz. The parameters for plotting the graph were taken as in the related experiment[8] and are given in Table I. In Fig. 3 the upper curves are shifted vertically for clarity. In Fig. 3(b) we plot the amplitude v versus the bias flux f_{dc} with the phenomenological lagging parameter $S=0.8$ for several values of the driving frequency ω, making use of Eqs. (27) and (28). In the experimental case the positions of these resonances at a given driving frequency allow one to determine the energy structure of the measured qubit.[8]

Figure 3 demonstrates the effect described in Sec. III: for $S\neq0$ both the phase shift α and the amplitude v depend on $\mathcal{L}^{-1}$, which results in the alternation of peak and dip around

the location of the resonances. We also note that, in addition, the terms nonlinear in S distort this structure. The second-order term, for example, is proportional to $\mathcal{L}^{-2}(3S^2-1)$. For values $S>1/\sqrt{3}$ this term leads to an increase in the peak and decrease in the dip leading to the asymmetry visible in the upper curve of Fig. 3(b).

In Fig. 4 we plot the phase shift α and the amplitude v as functions of the bias current frequency ω_{rf} and the flux detuning f_{dc} with the phenomenological lagging parameter S for the flux qubit with the parameters given in Table. I. The dashed white line shows the tank resonance frequency $\omega_{rf}/2\pi=\omega_T/2\pi=20.8$ MHz. Note that for the lagging parameter close to 1 ($S=0.8$) the changes in the phase shift in Fig. 4(a) are small at the resonance frequency (along the white line) while the voltage amplitude in Fig. 4(b) changes substantially. Such changes of the tank effective resistance, or equivalently, quality factor were studied in Ref. 9.

B. Landau-Zener interferometry

LZ interferometry is demonstrated in Fig. 5 as the dependence of the tank voltage phase shift α on the microwave amplitude f_{ac} and the dc flux bias f_{dc}. The qubit parameters were taken as in Fig. 3 (Table I) and $\omega/2\pi=4.15$ MHz.

The multiphoton resonances at discrete dc bias f_{dc} (which controls the distance between energy levels) are clearly visible. These resonances appear when the energy of n photons matches the qubit energy levels, $n\hbar\omega=\Delta E(f_{dc})$. Note also the quasiperiodical character of the dependence on the ac flux amplitude f_{ac}, which is known as Stückelberg oscillations; the comparison of such graph to the experimental analog[8] (namely, the estimation of the period of Stückelberg oscillations) allows the relation of the microwave power to the ac flux amplitude f_{ac} to be determined.

C. Impact of finite bias current

Consider the impact of the finite bias current on the tank response. When the bias current is small, its influence can be neglected and there is a peak-and-dip structure around the point where the qubit is resonantly excited to the upper state,
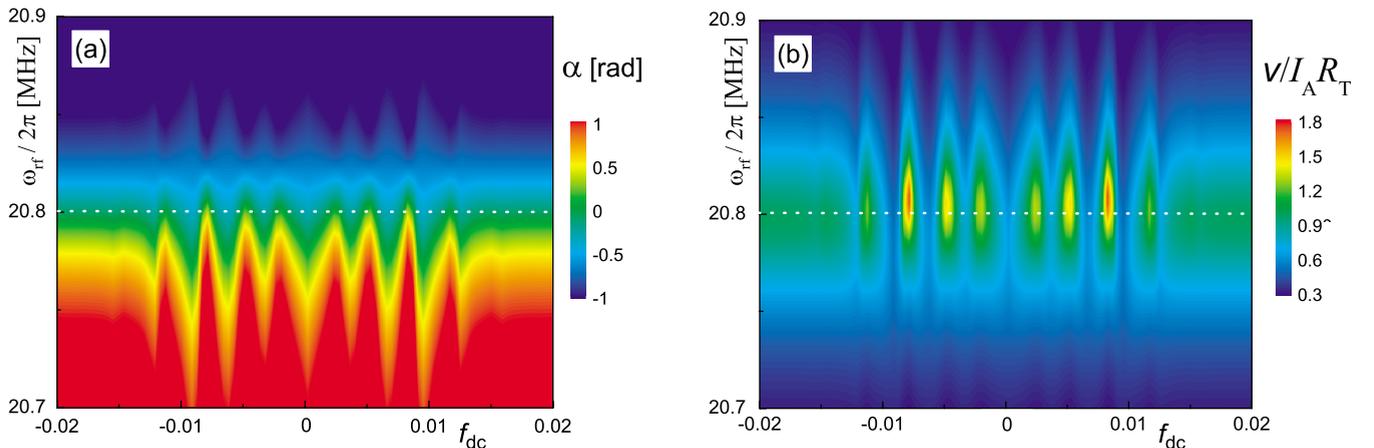
FIG. 4. (Color online) Multiphoton excitations of a single flux qubit. (a) Dependence of the phase shift α and (b) the amplitude v on the bias current frequency ω_{rf} and the flux detuning f_{dc}; the parameters are $f_{ac}=8\times10^{-3}$, $\omega/2\pi=4.15$ GHz, and $S=0.8$.
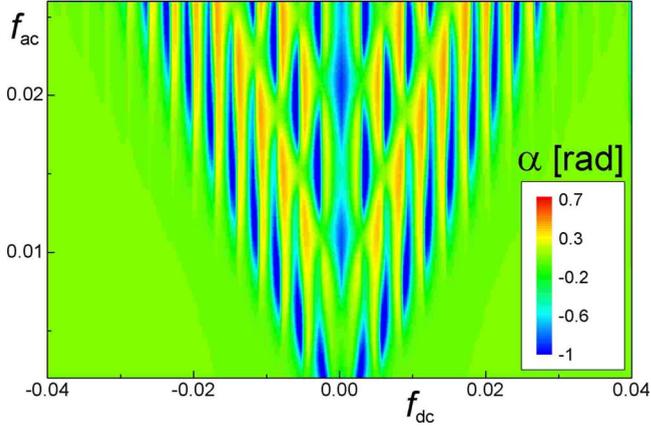
FIG. 5. (Color online) Landau-Zener interferometry: dependence of the tank phase shift on the flux detuning $f_{dc}=\Phi_{dc}/\Phi_0 -1/2$ and on the driving flux amplitude $f_{ac}=\Phi_{ac}/\Phi_0$.

see Eq. (22); these structures are distorted by the nonlinear terms when the current is increased. This is demonstrated in Fig. 6, where we plot the dependence of the phase shift α on the bias flux f_{dc} for two different values of the bias current amplitude I_A. The qubit parameters were taken as in Fig. 3 (Table. I).

VI. RESULTS FOR THE TWO-QUBIT SYSTEM

A. Resonant excitation

In this section we investigate the resonant excitation of a system of two coupled flux qubits. First we will describe the effects of resonant excitation in a system of two qubits in terms of its energy structure, entanglement measure, and the observable tank circuit phase shift. Then we will study the one-photon excitation of the system, which is used for the spectroscopic measurements. Finally we will demonstrate the multiphoton fringes. For calculations we will use the two sets of parameters as in Refs. 8 and 25 [denoted by (ii) and (i), respectively] which are given in Table II. Here, for clarity, we consider the case when the characteristic measurement time T is larger than the characteristic times of the dynamics of the qubit (T_1). Then the tank circuit actually probes the incoherent mixture of qubit's states and the time-averaged values of phase shift and entanglement should be considered. We calculate the energy levels (by diagonalizing the stationary Hamiltonian), the density matrix ρ, the observable tank circuit phase shift α (which is defined by the effective inductance of the qubits), and the entanglement measure $\mathcal{E}$ by making use of Eqs. (34)–(39). Then we plot Fig. 7 for the set of parameters (i) and the driving frequency
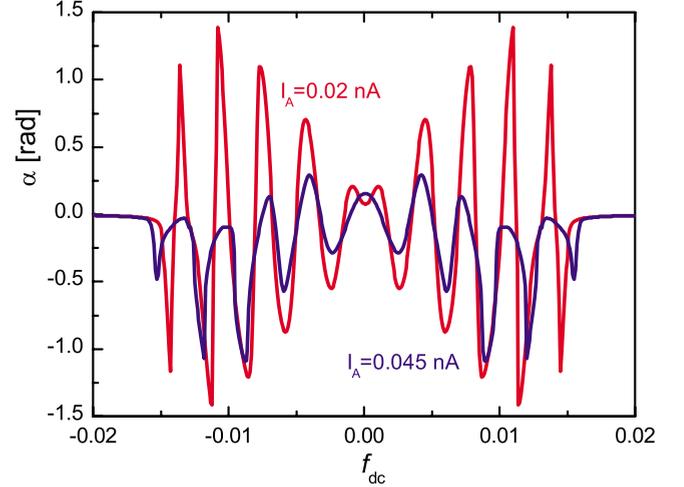
FIG. 6. (Color online) Impact of the finite bias current: dependence of the phase shift α on the bias flux f_{dc} for different values of the bias current amplitude I_A, for $\omega/2\pi=4$ GHz and $f_{ac}=8\times10^{-3}$.

$\omega/2\pi=4$ GHz, assuming the symmetrical change of the dc flux: $f_a=f_b\equiv f_{dc}$. Four energy levels are plotted in Fig. 7(a). When the energy of n photons ($n\hbar\omega$) matches the energy difference between any two levels E_j and E_i, the resonant excitation to the upper level is expected. With the green (gray), black, and magenta (dark gray) arrows of the lengths 4, 8, and 12 Ghz, respectively, we show the places of possible one-, two-, and three-photon excitations. The time-averaged total probability of the currents in two qubits that flow clockwise, $Z=R_{03}+R_{30}$, is shown in Fig. 7(b) to experience resonant excitation; black and red (dark gray) lines correspond to $f_{ac}=0$ and 10^{-3}. The resonances appear as hyperboliclike structures in the phase-shift dependence in Fig. 7(c). The time-averaged entanglement measure $\mathcal{E}$ has a peak in resonance [Fig. 7(d)]. The entanglement measure in a resonance increases due to the resonant formation of the superposition of states; this provides a tool for resonantly controlling the entanglement, and on the other hand comparing Figs. 7(c) and 7(d) is a method to probe the entanglement.

B. Spectroscopy (one-photon excitation)

A weakly driven system of qubits can be resonantly excited to an upper level when the driving frequency matches the distance between the energy levels. This can be used for the spectroscopic measurement of the energy structure of the system. In analogy to the related experiment[8] we plot in Fig. 8 the tank phase shift when the tank is coupled to the two flux qubits with the set of parameters (ii) and for the driving frequency and amplitude: $\omega/2\pi=17.625$ GHz and f_{ac}

TABLE II. The parameters of the two-qubit systems. All parameters are in units of h GHz except $\Xi_{a,b}$ which are dimensionless.

	Δ_a	Δ_b	$I_p^{(a)}\Phi_0$	$I_p^{(b)}\Phi_0$	J	Ξ_a	Ξ_b
(i)	1.1	0.9	990	990	0.84	1.8×10^{-3}	1.8×10^{-3}
(ii)	15.8	3.5	375	700	3.80	1.4×10^{-3}	2.6×10^{-3}
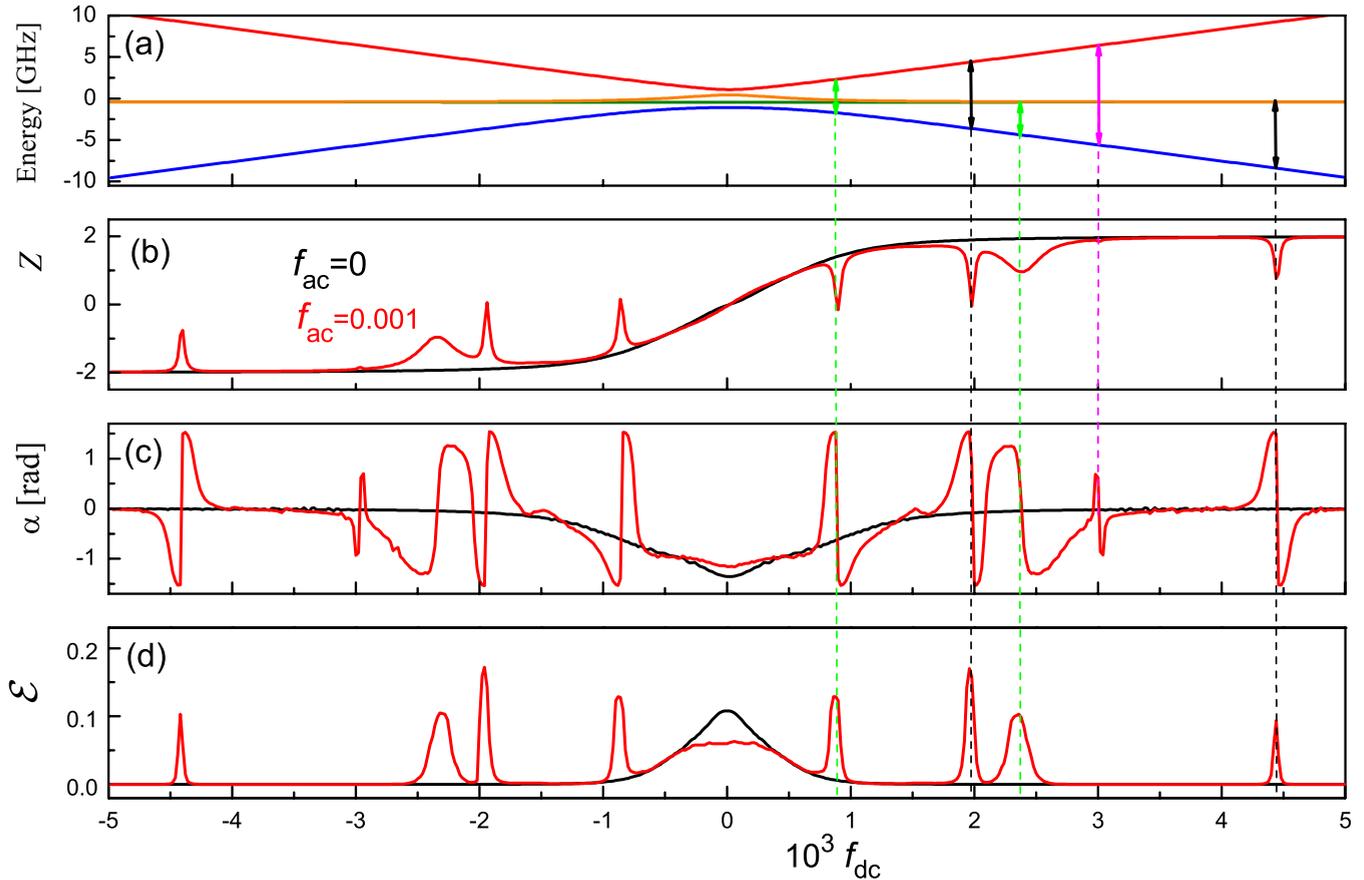
FIG. 7. (Color online) Multiphoton excitations of coupled flux qubits: (a) energy levels, (b) total probability of the currents in qubits to flow clockwise Z, (c) the tank phase shift α, and (d) the entanglement measure $\mathcal{E}$ versus the bias $f_{dc}=f_a=f_b$.

$=10^{-3}$. The resonances are visualized as the ridge-trough lines, as described above. The wide dip around $f_b \sim 0$ is due to the ground-state curvature. Solid lines are the energy contour lines which show where the photon energy $\hbar\omega$ matches the respective levels: ground and first excited (black), ground and second excited (white), and second excited and upper (third excited) levels (orange/gray).

An interesting situation arises when one photon excites the system to an intermediate level (to the second excited level in the figure); then, due to the nonzero level population, another photon can excite the system to a higher level (to the third excited level in the figure). This is shown with the white circle in Fig. 8, which marks the region where the signal is increased. The gray circle shows that such increase may not be visible when the former excitation (to the second excited level) creates such population (close to 1/2) that the tank signal is maximal.

C. Multiphoton excitations

When the qubits are strongly driven, excitations due to multiphoton processes become possible. In this case resonances appear where the energy-level difference is a multiple of the photon energy $\hbar\omega$. The multiphoton fringes are shown in Fig. 9 for the following driving and qubit parameters: (a) $\omega/2\pi=4$ GHz, $f_{ac}=5\times10^{-3}$, and the qubit parameters from (i); (b) $\omega/2\pi=4.15$ GHz and $f_{ac}=7\times10^{-3}$, and the qubit

parameters from (ii) with equal parameters (those for qubit a are taken to be the same as for qubit b: $\Delta_a=\Delta_b=3.5$, etc.).

The lines in Fig. 9(b) are the energy contour lines. They show that the multiphoton resonances are mostly due to the excitation to the first-excited level (black lines) with the in-
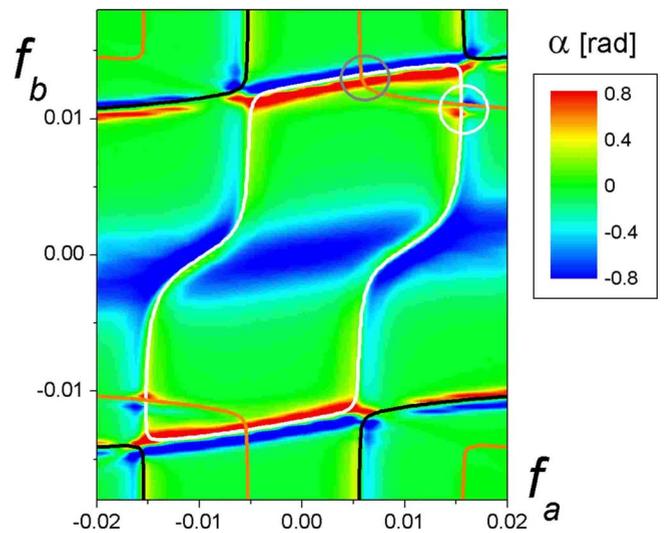
FIG. 8. (Color online) Resonant excitation of two coupled flux qubits: the tank phase shift versus partial bias fluxes in two qubits, f_a and f_b.
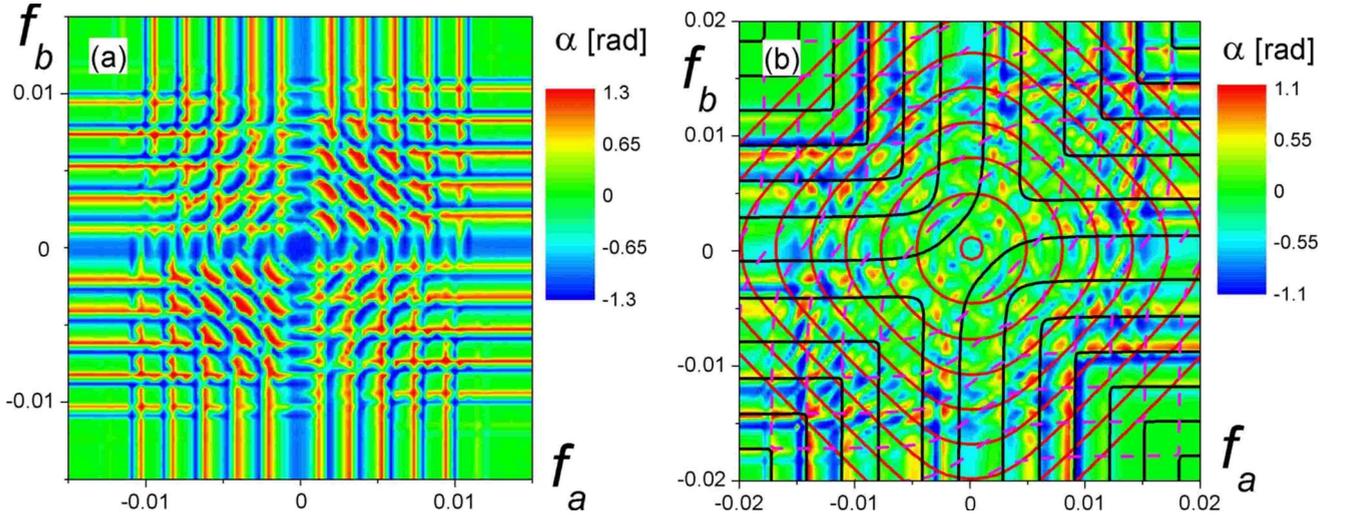
FIG. 9. (Color online) Multiphoton resonances in coupled qubits: dependence of the tank phase shift on the flux detuning in qubits a and b, f_a and f_b.

terruptions in ridge-trough resonant structures (change in the signal), where higher levels are matched with the multiple photon energy; possible excitations to the second excited level are shown with the magenta (dashed gray) line and to the upper level with the red (solid dark gray) line.

VII. RELATION TO EXPERIMENT

As mentioned above, experimental results related to Figs. 2, 3(b), and 5 were already reported in Refs. 8 and 39. The presented theory gives a good agreement with those experiments. Here we present some additional data obtained by making use of the same experimental procedure as in Ref. 8. In these experiments the tank circuit was realized as a parallel connection of a superconducting niobium coil and commercial ceramic capacitor (see Fig. 1). The superconducting persistent current qubits, three Josephson junctions closed into a superconducting ring,[10] were deposited by an aluminum shadow evaporation technique in the center of the su-

perconducting coil. The voltage across the tank circuit $V = v \exp(i\alpha)$ was amplified by a cryogenic amplifier and measured by an rf lock-in amplifier.

In Fig. 10 multiphoton resonances for a single qubit are shown in dependence of both the dc flux f_{dc} and the frequency of the driving current ω_{rf}. This data should be compared with the theoretical result presented in Fig. 4. Additional multiphoton lines, similar to the theoretical results of Fig. 3(a), are shown in Fig. 11(a). Those results were recorded at the resonant frequency only. Finally we studied the impact of finite bias current on the tank response as shown in Fig. 11(b) which should be compared with Fig. 6. Also in this more detailed comparison with the experiments, we find a good agreement with the theory presented in this work. Experimental results for the multiphoton resonances in coupled qubits will be published elsewhere.
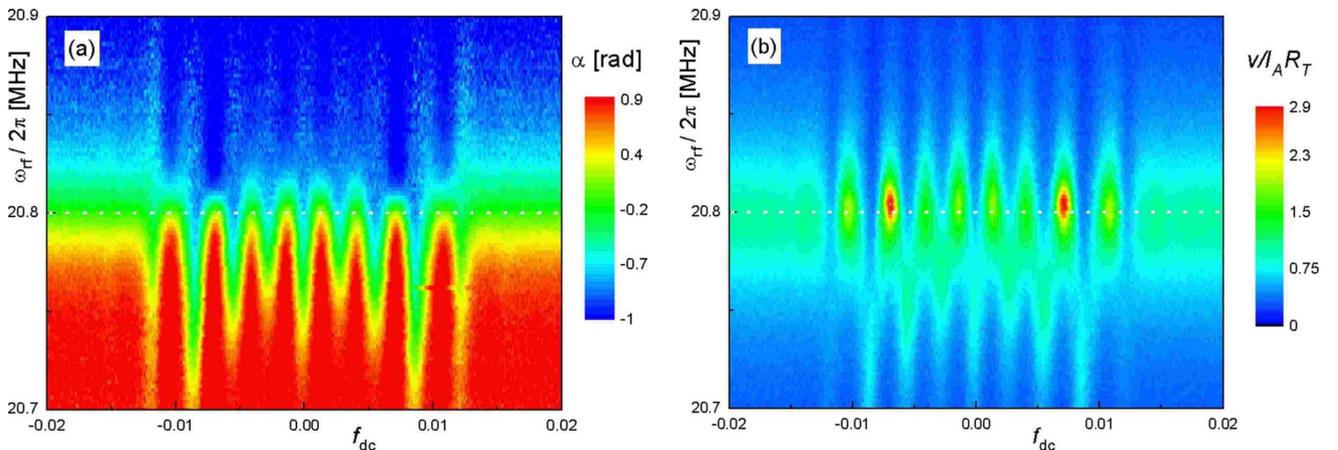
FIG. 10. (Color online) Experimental demonstration of multiphoton excitations in a single flux qubit. (a) Dependence of the phase shift α and (b) the amplitude v on the bias current frequency ω_{rf} and the flux detuning f_{dc} recorded for a microwave excitation with $\omega/2\pi = 4.15$ GHz and amplitude $f_{ac} = 4.5 \times 10^{-3}$.
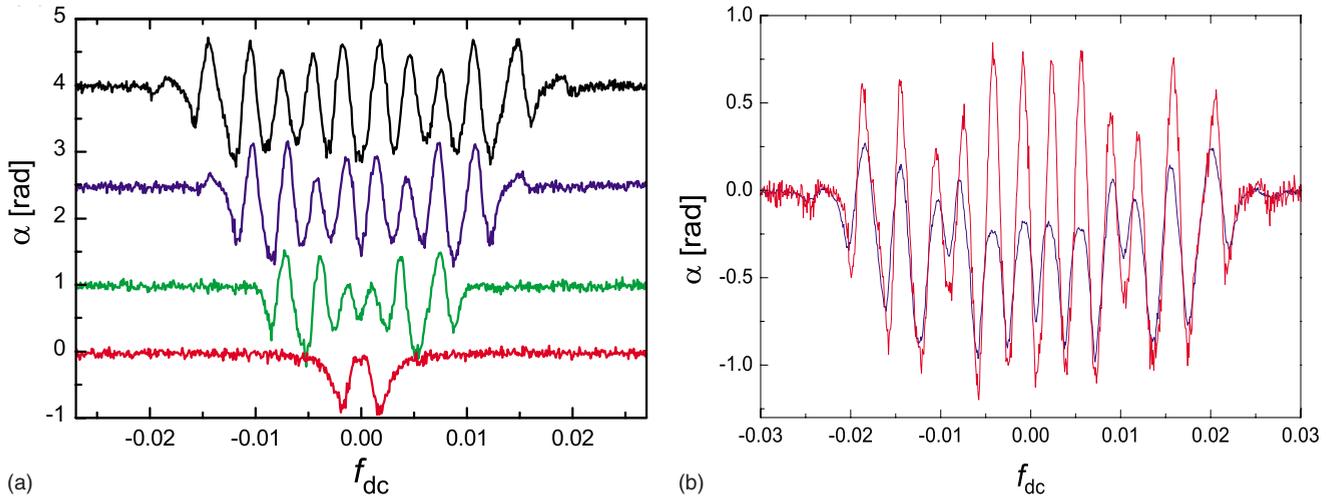
FIG. 11. (Color online) Experimental dependence of the phase shift α on the bias flux f_{dc}: (a) multiphoton resonances for driving amplitudes $f_{ac}/10^{-3}=0.5$, 2.5, 4.5, and 6.5 from top to bottom; (b) influence of the bias current (red line $I_A M/\Phi_0=2\times 10^{-6}$ and blue line $I_A M/\Phi_0=8\times 10^{-6}$) for $\omega/2\pi=4.15$ GHz.

VIII. CONCLUSION

The application of the impedance measurement technique for monitoring resonant excitations in flux qubits was studied. It was shown that excitation of the qubits change their effective inductance. This results in a changed effective inductance and resistance of the tank circuit. Thus, the observable quantities—the amplitude and phase shift of the tank voltage—reflect the changes in the effective inductances of the qubits. Transparent expressions were derived in two limiting cases: one where the dynamics of the tank is slow relative to the time scale of the qubits and another where both time scales are of the same order. In the first case the changes in the tank resistance are negligible and the phase shift is directly related to the effective inductance. It has also been demonstrated that in the latter case both the effective inductance and resistance of the tank are defined by the inductance of the qubit. Our theoretical analysis describes the state of the system of qubits in terms of the tank effective inductance and resistance. This allowed us to describe the experimental results on multiphoton resonant excitation of single and coupled qubits.

The impact of the finite bias current and of the temperature was described as well. In particular it was shown that the thermal excitation of the qubit to the upper-level results in the widening of the dip visible in the phase shift, as was observed previously in the experiment.[39]

The resonant excitation of qubits can be used not only for controlling their state but also for determining their parameters. The developed theory has been used to reproduce the experimental results presented in Ref. [8] for single qubits and pairs of coupled flux qubits. In addition to single-photon ("spectroscopic") resonances we have shown the appearance of the multiphoton excitations in flux qubits coupled to the tank circuit.

[1] J. M. Raimond, M. Brune, and S. Haroche, Rev. Mod. Phys. **73**, 565 (2001).

[2] A. Wallraff, D. I. Schuster, A. Blais, L. Frunzio, R.-S. Huang, J. Majer, S. Kumar, S. M. Girvin, and R. J. Schoelkopf, Nature (London) **431**, 162 (2004).

[3] E. Il'ichev, N. Oukhanski, A. Izmalkov, Th. Wagner, M. Grajcar, H.-G. Meyer, A. Yu. Smirnov, A. Maassen van den Brink, M. H. S. Amin, and A. M. Zagoskin, Phys. Rev. Lett. **91**, 097906 (2003).

[4] E. Il'ichev, N. Oukhanski, Th. Wagner, H.-G. Meyer, A. Yu. Smirnov, M. Grajcar, A. Izmalkov, D. Born, W. Krech, and A. Zagoskin, Low Temp. Phys. **30**, 620 (2004).

[5] D. Born, V. I. Shnyrkov, W. Krech, Th. Wagner, E. Il'ichev, M. Grajcar, U. Hübner, and H.-G. Meyer, Phys. Rev. B **70**, 180501(R) (2004).

[6] A. Lupascu, C. J. P. M. Harmans, and J. E. Mooij, Phys. Rev. B **71**, 184506 (2005).

[7] V. I. Shnyrkov, Th. Wagner, D. Born, S. N. Shevchenko, W.

Krech, A. N. Omelyanchouk, E. Il'ichev, and H.-G. Meyer, Phys. Rev. B **73**, 024506 (2006).

[8] A. Izmalkov, S. H. W. van der Ploeg, S. N. Shevchenko, M. Grajcar, E. Il'ichev, U. Hübner, A. N. Omelyanchouk, and H.-G. Meyer, Phys. Rev. Lett. **101**, 017003 (2008).

[9] M. Grajcar, S. H. W. van der Ploeg, A. Izmalkov, E. Il'ichev, H.-G. Meyer, A. Fedorov, A. Shnirman, and G. Schön, Nat. Phys. **4**, 612 (2008).

[10] J. E. Mooij, T. P. Orlando, L. Levitov, L. Tian, C. H. van der Wal, and S. Lloyd, Science **285**, 1036 (1999).

[11] A. Yu. Smirnov, Phys. Rev. B **68**, 134514 (2003).

[12] Ya. S. Greenberg, E. Il'ichev, and A. Izmalkov, Europhys. Lett. **72**, 880 (2005).

[13] Ya. S. Greenberg and E. Il'ichev, Phys. Rev. B **77**, 094513 (2008).

[14] J. Hauss, A. Fedorov, C. Hutter, A. Shnirman, and G. Schön, Phys. Rev. Lett. **100**, 037003 (2008).

[15] A. B. Zorin, Physica C **368**, 284 (2002).

[16] W. Krech, M. Grajcar, D. Born, I. Zhilyaev, Th. Wagner, E. Il'ichev, and Ya. Greenberg, Phys. Lett. A **303**, 352 (2002).

[17] Ya. S. Greenberg, A. Izmalkov, M. Grajcar, E. Il'ichev, W. Krech, H.-G. Meyer, M. H. S. Amin, and A. Maassen van den Brink, Phys. Rev. B **66**, 214525 (2002).

[18] Ya. S. Greenberg, A. Izmalkov, M. Grajcar, E. Il'ichev, W. Krech, and H.-G. Meyer, Phys. Rev. B **66**, 224511 (2002).

[19] S. N. Shevchenko, Eur. Phys. J. B **61**, 187 (2008).

[20] A. V. Shytov, D. A. Ivanov, and M. V. Feigel'man, Eur. Phys. J. B **36**, 263 (2003).

[21] M. Sillanpää, T. Lehtinen, A. Paila, Yu. Makhlin, and P. Hakonen, J. Low Temp. Phys. **146**, 253 (2007).

[22] W. D. Oliver, Ya. Yu, J. C. Lee, K. K. Berggren, L. S. Levitov, and T. P. Orlando, Science **310**, 1653 (2005).

[23] S. N. Shevchenko and A. N. Omelyanchouk, Low Temp. Phys. **32**, 973 (2006).

[24] S. Ashhab, J. R. Johansson, A. M. Zagoskin, and F. Nori, Phys. Rev. A **75**, 063414 (2007).

[25] A. Izmalkov, M. Grajcar, E. Il'ichev, Th. Wagner, H.-G. Meyer, A. Yu. Smirnov, M. H. S. Amin, A. Maassen van den Brink, and A. M. Zagoskin, Phys. Rev. Lett. **93**, 037003 (2004).

[26] J. B. Majer, F. G. Paauw, A. C. J. ter Haar, C. J. P. M. Harmans, and J. E. Mooij, Phys. Rev. Lett. **94**, 090501 (2005).

[27] A. O. Niskanen, K. Harrabi, F. Yoshihara, Y. Nakamura, and J. S. Tsai, Phys. Rev. B **74**, 220503(R) (2006).

[28] Yu-xi Liu, L. F. Wei, J. S. Tsai, and F. Nori, Phys. Rev. Lett. **96**, 067003 (2006).

[29] J. H. Plantenberg, P. C. de Groot, C. J. P. M. Harmans, and J. E. Mooij, Nature (London) **447**, 836 (2007).

[30] Y. Yu, W. D. Oliver, J. C. Lee, K. K. Berggren, L. S. Levitov, and T. P. Orlando, arXiv:cond-mat/0508587 (unpublished).

[31] N. N. Bogolyubov and Yu. A. Mitropol'skii, *Asymptotic Methods in the Theory of Nonlinear Oscillations* (Gordon and Breach, New York, 1962 / Nauka, Moscow, 1974).

[32] C. H. Metzger and K. Karral, Nature (London) **432**, 1002 (2004).

[33] J. Schlienz and G. Mahler, Phys. Rev. A **52**, 4396 (1995).

[34] P. J. Love, A. Maassen van den Brink, A. Yu. Smirnov, M. H. S. Amin, M. Grajcar, E. Il'ichev, A. Izmalkov, and A. M. Zagoskin, Quantum Inf. Process. **6**, 187 (2007).

[35] E. A. Ivanchenko, Low Temp. Phys. **33**, 336 (2007).

[36] M. Grajcar, A. Izmalkov, S. H. W. van der Ploeg, S. Linzen, E. Il'ichev, Th. Wagner, U. Hübner, H.-G. Meyer, A. Maassen van den Brink, S. Uchaikin, and A. M. Zagoskin, Phys. Rev. B **72**, 020503(R) (2005).

[37] K. Blum, *Density Matrix Theory and Applications* (Plenum, New York, 1981).

[38] S. N. Shevchenko, A. S. Kiyko, A. N. Omelyanchouk, and W. Krech, Low Temp. Phys. **31**, 569 (2005).

[39] M. Grajcar, A. Izmalkov, E. Ilichev, T. Wagner, N. Oukhanski, U. Hübner, T. May, I. Zhilyaev, H. E. Hoenig, Y. S. Greenberg, V. I. Shnyrkov, D. Born, W. Krech, H. G. Meyer, A. Maassen van den Brink, and M. H. S. Amin, Phys. Rev. B **69**, 060501(R) (2004).